First-principles study of 180° domain walls in $BaTiO_3$: Mixed Bloch-Néel-Ising character

Menglei Li,[1,2,3] Yijia Gu,[2] Yi Wang,[2] Long-Qing Chen,[2,4] and Wenhui Duan[1,3,*]

[1]*Department of Physics and State Key Laboratory of Low-Dimensional Quantum Physics, Tsinghua University, Beijing 100084, People's Republic of China*

[2]*Department of Materials Science and Engineering, Pennsylvania State University, University Park, Pennsylvania 16802, USA*

[3]*Collaborative Innovation Center of Quantum Matter, Tsinghua University, Beijing 100084, People's Republic of China*

[4]*School of Materials Science and Engineering, Tsinghua University, Beijing 100084, People's Republic of China*

(Received 5 March 2014; revised manuscript received 10 July 2014; published 13 August 2014)

The 180° ferroelectric domain walls (FDWs) have long been regarded as purely Ising type in ferroelectrics, but recent theoretical works suggested that they can also have Néel- and/or Bloch-like rotations. Using a combination of first-principles calculations with phase-field simulations, we studied the 180° FDWs on different crystallographic planes in prototypical ferroelectric perovskite $BaTiO_3$. The polarization profiles of 180° FDWs on (100) and (410) planes revealed that the (100)- and (410)-FDWs both exhibit Néel-like character besides their intrinsic Ising character, while the (410)-FDW also simultaneously shows a Bloch-like oblique of ∼6 nm, as a consequence of the deviation of polarization gradient from the high symmetry direction. Due to the existence of the Néel-like component of polarization, 180° FDWs in $BaTiO_3$ exhibit a multilayer charge redistribution and thus may strongly trap charged defects.

DOI: 10.1103/PhysRevB.90.054106 PACS number(s): 77.80.Dj, 31.15.E−, 77.22.Ej, 77.84.−s

I. INTRODUCTION

Ferroelectricity is a property of materials with spontaneous electric polarization that can be switched by an external electric field [1]. Ferroelectrics has received tremendous attention for their applications in memory storage devices [2–4]. Available ferroelectric crystals are inevitable to contain domains with different orientations of the polarization [5]. Upon applying sufficient external electric field, the orientations of different domains can rotate to align along the field, thus domains merge and domain walls (i.e., the boundary between two different-oriented domains [6]) disappear. In this way ferroelectric domain structures affect the macroscopic response of the devices [7]. Therefore, domain walls, as an important part of domain structure, have been intensively studied, including the domain wall dynamics under external field [8–11], domain wall conductivity [12–15], and interaction between domain wall and various defects (including oxygen vacancy and pinning effect) [14,16–18].

180° ferroelectric domain walls (FDWs), which divide two domains with antiparallel polarization orientations, are common in ferroelectric crystals [11]. They have long been considered as charge-neutral Ising-type domain wall across which the polarization simply reverses its direction over several atomic layers [19]. Recent theoretical and experimental studies [20–28], however, revealed that the polarization in the 180° FDWs can also simultaneously rotate in a plane normal to the domain wall or parallel to the domain wall, which is called Néel-like or Bloch-like character borrowed from the magnetic domain wall [29]. This suggests that the previously accepted view of 180° FDWs needs to be refined. First-principles-based Monte Carlo simulations found that ultrathin $Pb(Zr_{0.5}Ti_{0.5})O_3$ films show a vortex stripe domain structure [26,27], while atomistic simulations based on Ginzburg-Landau-Devonshire (GLD) theory showed that the polarization across the FDW in hexagonal $LiNbO_3$ has both Bloch- and Néel-like oblique [22]. Moreover, in perovskite crystal ferroelectrics, which are one of the most important families of ferroelectric materials, 180° FDWs have been demonstrated to show Ising character mixed with Bloch- or Néel-like fluctuations by several groups [20,23,24]. And 180° FDWs in pure tetragonal phase $PbTiO_3$ (PT) were found to be of Ising-Néel-like type [23], with the Néel-like component reaching 2.16 $\mu C/cm^2$ (∼2.5% of the bulk polarization) [20]. In contrast, 180° FDWs in rhombohedral $BaTiO_3$ (BT) have combined Ising-Bloch-like nature [24]. Furthermore, GLD theoretical modeling [25] suggested that in the presence of flexoelectric coupling, i.e., the interaction between strain gradient and the order parameter, 180° FDWs in tetragonal BT are bichiral in their notation which have a Bloch oblique of the order 10^{-2} $\mu C/cm^2$ except (110) and (100) walls, whereas the Néel-like component is screened by the depolarization field. However, there have been no observation of FDWs that simultaneously possess both the Bloch- and Néel-like components in existing studies of tetragonal perovskite-type ferroelectrics.

In this work we investigate 180° FDWs in tetragonal BT using first-principles calculations combined with phase-field simulations. One of objectives is to understand if a FDW can simultaneously have the three characters, i.e., Ising, Néel-like, and Bloch-like characters. We choose a domain wall lying in (410) crystallographic plane mainly because the domain wall of $\theta = \pi/12$ with respect to the crystallographic lattice plane $\{100\}$ was theoretically predicted to have the largest Bloch-like component [25] and the (410)-FDW of $\theta = 14°$ is the closest configuration. It is noted that 180° (410)-FDW has never been studied using the density functional theory (DFT). Our calculations show that this (410)-domain wall indeed has mixed Ising-Bloch-Néel-like nature. Another objective is to revisit and validate the GLD-theory-based conclusions by using the first-principles method. First-principles calculations require no empirical parameters and thus may provide quantitatively correct results for real materials. In comparison

*dwh@phys.tsinghua.edu.cn

to the results from GLD theory [25], our first-principles calculations show that the Néel-like component exists and the Bloch-like component is 100 times larger in 180° (410)-FDW of BT, whereas the variation trend of Néel-like and Bloch-like components across the domain wall is qualitatively confirmed by performing phase-field modeling.

The rest of the paper is organized as follows. First, we describe how we construct our FDW configurations in Sec. II. Then the details of first-principles calculations as well as phase-field model are provided in Sec. III. In Sec. IV we present our results of 180° FDW in the (100) plane and (410) plane of BT together with detailed discussions on physical mechanism. At the end we give a brief summary in Sec. V.

II. FDW GEOMETRY AND CONFIGURATIONS

Barium titanate ($BaTiO_3$) crystallizes in the rhombohedral structure at 0 K [30]. With increasing temperature, it undergoes structural transitions from this phase to orthorhombic phase, then to tetragonal phase where the direction of the spontaneous polarization rotates to the [001] pseudocubic direction [as shown in Fig. 1(b)], and finally to a paraelectric cubic phase [30]. The present work focuses on the tetragonal ferroelectric phase of BT, which is stable at room temperature. In fact, there exist quite a few first-principles studies published on the tetragonal phase of BT [31,32], showing that DFT calculation can have good accuracy regarding most of the physical properties of this phase.

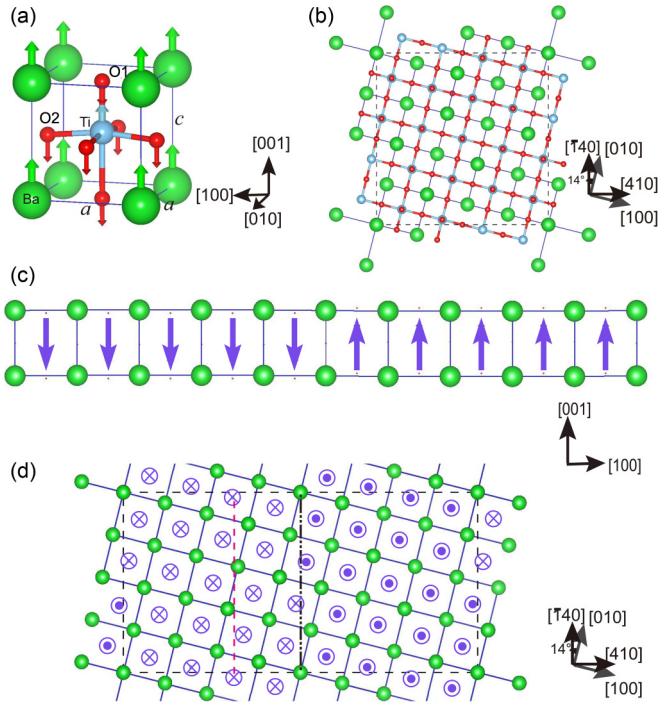

FIG. 1. (Color online) (a) Unit cell of tetragonal BT which is used as a building unit of (100)-FDW, with polarization along the [001] direction. Arrows represent the atomic displacements from nonpolarized centrosymmetric positions. (b) A building unit for (410)-FDW. (c) Supercell geometry of the (100)-FDW which contains 10 unit cells. (d) (410)-FDW geometry. Black (red) dot-dashed (dashed) line indicates BaO (TiO)-centered plane.

Experimental investigations have indicated that 180° FDWs in BT can lie in any direction due to the low anisotropy energy [6], while previous theoretical focus has mainly been on (100)- and (110)-FDWs [24,33]. Therefore, we first calculate structural and polarization distributions of BT (100)-FDWs, along with a comparison with those of PT [33], and explore the existence of Néel-like character for the FDWs in BT. Then we consider a (410)-FDW which has not been studied before. Our model structures consist of [001]-oriented domains separated by FDWs. To build the supercell model for FDWs along a certain direction, we repeat the unit cell [shown in Figs. 1(a) and 1(b)] N times along the direction normal to the FDW. With the imposed periodical boundary conditions, the supercell contains two equivalent FDWs with one being in the middle and the other being in the ends. The interaction between these two domain walls should be minimized or eliminated by stacking enough unit cells between them. We test the number of unit cells in (100)-FDW configuration until the domain wall energy reaches convergence. For the (410)-FDW, the smallest configuration contains 34 primitive cells and the distance between two domain walls is naturally large enough.

For (100)-FDWs we stack the relaxed five-atom tetragonal cell in the direction normal to the FDW to form a supercell consisting of $2N \times 1 \times 1$ unit cells ($N = 4, 5, \ldots, 8$). Then we set the initial polarizations to obtain a pure Ising-type FDW (i.e., the opposite polarizations with only P_z component on the two sides of the domain wall). Note that the domain wall can lie on either BaO plane or TiO plane, and thus one Ba atom or Ti atom on this particular plane is set as the inversion center. This structural symmetry will be kept in the first-principles calculations, which is a general practice in the study of systems with extended defects such as grain boundary and domain wall [19,33–35]. Figure 1(c) shows an $N = 5$ BaO-centered FDW.

For the (410)-FDW the minimal building unit is an 85-atom cell as shown in Fig. 1(b), obtained by expanding the dimensions of the relaxed five-atom primitive cell to $\sqrt{17} \times \sqrt{17} \times 1$ times. The lattice vectors of this cell are $(4a, a, 0)$, $(-a, 4a, 0)$, and $(0, 0, c)$, respectively, where a and c are the calculated lattice parameters of tetragonal BT phase. Putting two building units, or domains, with opposite polarization orientations together as shown in Fig. 1(d), we get the 180° FDWs in the (410) direction. Similar to the (100)-FDWs, the (410)-FDW can center on either the BaO plane or TiO plane. And we also put the inversion center of the structure on the Ba or Ti atom of the center plane of the FDW. The two kinds of lattice planes are marked in Fig. 1(d).

III. COMPUTATIONAL DETAILS

We carry out first-principles calculations based on DFT, as implemented in the Vienna *ab initio* simulation package (VASP) [36]. The wave functions are expanded in plane waves up to an energy cutoff of 400 eV (note: increasing the energy cutoff to 520 eV yields little difference in the total energy and atomic structure). We employ the projector augmented-wave pseudopotentials [37,38] with the generalized gradient approximation (GGA) of PBEsol functional [39]. Ba($5s$, $5p$,

TABLE I. Materials parameters of $BaTiO_3$ in phase-field simulation. The values of parameters are collected and recalculated from Ref. [46] if not indicated otherwise. Other sources of the parameters can be found from the superscript characters. The phase-field simulations are performed under 298 K.

Coefficients	Values
$\varepsilon_b, \varepsilon_0$	$\varepsilon_b = 45$,[a] $\varepsilon_0 = 8.85 \times 10^{-12}$
a_i (C^{-2} m J)	$a_1 = 5 \times 10^5\ T_S[\coth(\frac{T_s}{T}) - \coth(\frac{T_s}{390})]$, $T_s = 160$ K
a_{ij} ($\times 10^8$ C^{-4} m^5 J)	$a_{11} = -1.154$, $a_{12} = 6.53$
a_{ijk} ($\times 10^9$ C^{-6} m^9 J)	$a_{111} = -2.106$, $a_{112} = 4.091$, $a_{123} = -6.688$
a_{ijkl}($\times 10^{10}$ C^{-8} m^{13} J)	$a_{1111} = 7.59$, $a_{1112} = -2.193$, $a_{1122} = -2.221$, $a_{1123} = 2.416$
Q_{ij} (C^{-2} m^4)	$Q_{11} = 0.11$, $Q_{12} = -0.045$, $Q_{44} = 0.059$
s_{ij} ($\times 10^{-12}$ Pa^{-1})	$s_{11} = 9.07$, $s_{12} = -3.19$, $s_{44} = 8.2$
g_{ij} ($\times 10^{-10}$ C^{-2} m^3 J)	$g_{11} = 5.1$, $g_{12} = -0.2$, $g_{44} = 0.2$[b]
F_{ij} ($\times 10^{-11}$ C^{-1} m^3)	$F_{11} = 0.3094$, $F_{12} = -0.279$, $F_{44} = -0.1335$ (recalculated from c)

[a]Reference [47].
[b]Reference [48].
[c]Reference [49].

and 6s) electrons, Ti(3s, 3p, 3d, and 4s) electrons, and O(2s and 2p) electrons are treated as valence states. The geometry optimization is achieved under symmetry constraint [40] by the conjugate gradient algorithm [41] until the residual forces are smaller than 0.01 eV/Å [42]. Meanwhile, to consider stress introduced by the FDW we allow the length of supercell vector normal to the FDW to relax. A $1 \times 9 \times 9$ Monkhorst-Pack k mesh is used for the (100)-FDW and a $1 \times 3 \times 7$ k mesh is used for the (410)-FDW. In order to determine the domain wall energy, we construct a reference structure by aligning the polarizations of the two domains parallel in the supercell, corresponding to a single domain without FDW. Then with exactly the same k mesh and other settings we calculate the total energy of the reference structure and subtract it from the total energy of the supercell with domain walls.

We also calculate the Born effective charges of bulk tetragonal BT using density functional perturbation theory (DFPT) [43] as implemented in VASP. From these charge tensors we calculate the local polarizations and map the polarizations onto Ti atoms, where the algorithm proposed by Meyer and Vanderbilt [33] is adopted. There are eight nearest Ba atoms and six nearest O atoms for a Ti atom. The center of the eight Ba atoms is chosen as the reference position, and then the polarization mapping on Ti atoms can be computed as

$$\mathbf{P}_k = \frac{e}{\Omega_k}\left[\left(\boldsymbol{u}_k^{\mathrm{Ti}} - \boldsymbol{u}_{k_0}\right) \bullet Z_{Ti}^* + \frac{1}{2}\sum_{i=1}^{6}\left(\boldsymbol{u}_{k_i}^{\mathrm{O}} - \boldsymbol{u}_{k_0}\right) \bullet Z_O^* + \frac{1}{8}\sum_{j=1}^{8}\left(\boldsymbol{u}_{k_j}^{\mathrm{Ba}} - \boldsymbol{u}_{k_0}\right) \bullet Z_{Ba}^*\right], \quad (1)$$

where k indexes the Ti-centered unit cell, $\boldsymbol{u}_{k_0}$ is the central position of the cell, k_i and k_j are the indexes of oxygen and barium atoms, $\boldsymbol{u}$ is the atomic position, and Z^* is the Born effective charge tensor.

As complementary to the DFT calculations, we further perform phase-field simulations with the flexoelectric contribution [44]. Since the stress-free boundary condition is applied, it is more convenient to use Gibbs free energy [45], i.e.,

$$G = \alpha_{ij}P_iP_j + \alpha_{ijkl}P_iP_jP_kP_l + \alpha_{ijklmn}P_iP_jP_kP_lP_mP_n + \frac{1}{2}g_{ijkl}\frac{\partial P_i}{\partial x_j}\frac{\partial P_k}{\partial x_l} - \frac{1}{2}s_{ijkl}\sigma_{ij}\sigma_{kl} - Q_{ijkl}\sigma_{ij}P_kP_l + \frac{F_{ijkl}}{2}\left(\frac{\partial P_k}{\partial x_l}\sigma ij - \frac{\partial \sigma_{ij}}{\partial x_l}P_k\right) - P_i\left(E_i + \frac{E_i^d}{2}\right), \quad (2)$$

where P_i is the polarization component, σ_{ij} is the stress component, E_i and E_i^d are the applied electric field and the depolarization field, respectively, α's are the dielectric stiffness tensors, g_{ijkl} is the gradient energy coefficient, s_{ijkl} is the elastic compliance tensor, Q_{ijkl} is the electrostrictive tensor, and F_{ijkl} is the flexoelectric tensor. The values of the coefficients for BT are listed in Table I, taken from the literature [46–49]. The setup of the simulation is schematically illustrated in Fig. 2, where the angle θ represents the rotation angle of the FDW with respect to the crystallographic direction. The direction normal to the FDW is defined as x_n, and the pseudocubic [001] direction and the direction perpendicular to it within the wall plane are respectively defined as x_z and x_t (right handed). The system is then simplified to a one-dimensional problem with the simulation

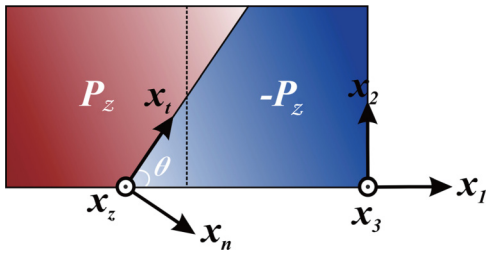

FIG. 2. (Color online) Schematic of the setup in the phase-field simulation. The oblique line represents the 180° FDW, which divides the area into two domains with opposite polarizations along the (001) direction (red and blue areas correspond to $+P_z$ and $-P_z$, respectively). Herein x_1, x_2, and x_3 refer to the crystallographic orientations [100], [010], and [001], respectively; while x_n, x_z, and x_t refer to, respectively, the direction normal to the FDW, the [001] direction and its perpendicular direction within the wall plane.

TABLE II. Calculated Born effective charges (in units of the charge quantum e) of Ba, Ti, and O atoms in tetragonal (in Cartesian coordinates) and cubic $BaTiO_3$ phases.

Tetragonal				Cubic	
Atom	Z^*_{xx}	Z^*_{yy}	Z^*_{zz}	Atom	Z^*
Ba	2.73	2.73	2.84	Ba	2.75
Ti	7.09	7.09	5.69	Ti	7.47
O1	−2.01	−2.01	−4.64	O	−2.15 ($O_\perp$) −5.86 ($O_\parallel$)
O2	−2.34	−5.98	−2.04		

size $4096\Delta x \times \Delta x \times \Delta x$, where Δx is the grid spacing. Periodical boundary condition is imposed along each direction. The stress of each grid point is calculated using Kachaturyan's microelastic theory [50], and the electric depolarization field is obtained by solving Poisson's equation. We start from a double-domain structure with only spontaneous $+P_z$ and $-P_z$ in each domain as illustrated in Fig. 2, and then relax the system to equilibrium.

IV. RESULTS AND DISCUSSION

As a starting point we first discuss the DFT results on the structural and ferroelectric properties of bulk tetragonal $BaTiO_3$ phase. The optimized structural parameters are $a = 3.9799$ Å, $c = 4.0768$ Å, in good agreement with the experimental values of $a = 3.9970$ Å, $c = 4.0314$ Å [51,52]. The calculated Born effective charges for each atom along three pseudocubic orientations are given in Table II, together with those of cubic phase. It can be seen that Z^* of Ba is almost isotropic, and the value is nearly the same for the cubic and tetragonal phases. However, compared with cubic phase, the Born effective charges of other atoms along the [001] direction significantly change by more than $1e$ (Z^*_{zz} of Ti is $5.69e$ compared to $7.47e$ and Z^*_{zz} of O1 is $-4.64e$ compared to $-5.86e$). Since the Ti-O bond length is varied along the [001] direction from cubic to tetragonal phase, dynamic charge transfer occurs. The calculated Born effective tensors meet closely with previous theoretical values. For the bulk tetragonal $BaTiO_3$, a polarization of 29.9 $\mu C/cm^2$ is achieved using the Born effective charges, which is in good agreement with the experimental value (26 $\mu C/cm^2$) [53].

A. 180° (100)-FDW

We analyze the system in terms of domain wall energy and polarization profile. As shown in Table III, BaO-centered (100)-FDW is lower in energy by about 70 mJ/m^2 than the TiO-centered one. Such a remarkable energy difference, which is almost independent of the supercell size used in the calculations, indicates that BaO-centered domain wall is generally more stable, consistent with previous first-principles based Monte Carlo simulations [19]. Importantly, it is found that the polarization profiles have similar trends for BaO-centered and TiO-centered domain walls, i.e., the presence of Néel-like nature does not depend on which plane the FDW centers on. Thus, we will focus on the ferroelectric properties of BaO-centered FDWs in the following.

TABLE III. Calculated 180° domain wall energies in units of mJ/m^2. Herein N is the number of the unit cells in the supercell for the (100)-FDW of $BaTiO_3$.

	(100)-FDW $N=$				(410)-FDW	(4$\bar{1}$0)-FDW
	5	6	7	8		
BaO-centered	14.10	15.18	14.68	14.81	18.98	13.21
TiO-centered	84.48	85.95	85.36	85.53	38.67	38.78

Figure 3(a) shows calculated polarization profile for BaO-centered (100)-FDW with $N = 8$. The polarization profile is certainly periodic due to the imposed periodic geometry of the supercell (one should note that both the edge and the center of the supercell are FDWs). The P_z component is zero in the center, but it recovers to the bulk value within one layer away from the domain wall, showing that the Ising domain wall width is less than 1 nm. But the profile of the P_n component manifests that the domain wall turns into an approximately 2 nm wide "Néel wall." The P_n component exhibits a tail-to-tail-like distribution inside the FDW while it remains zero outside the FDW. The widths are in good agreement with experimental values by Jia *et al.* [12] and Landau theory results from Gureev *et al.* [54], where the width of a "head-to-head" or "tail-to-tail" domain wall with nonzero bound charge was found to be about 10 unit cells while the width of a neutral domain wall is about 1 unit cell. Although the maximum value of P_n is only 0.11 $\mu C/cm^2$, comparable to that of 180° FDWs in $LiNbO_3$ [22], the P_n profiles of all the configurations we have calculated show the same trend instead of randomness. Moreover, in a single domain with no symmetry constraints, P_n would arise only as small as 5%–10% of P_n in FDW structures, indicating an intrinsic Néel-like character. By checking the atomic positions we find that all the neighborhood atoms except the O1 atom closest to the center of the wall move away from the FDW. The displacements of O atoms are 0.001–0.002 Å, while Ti atom jumps outward by 0.006 Å. As for the atoms in the next nearest neighbored layers and at further positions, their displacements become smaller and quickly converge to zero. Therefore the polarizations distribute in the form of tail-to-tail in the domain wall.

Just like in tetragonal BT, previous DFT studies on 180° (100)-FDW in PT have demonstrated that the P_n component also exists and shows a tail-to-tail-like distribution [20,23]. What is more, the width is nearly the same as that of FDW in BT. This suggests that the existence of mixed Ising-Néel-like FDWs is general in perovskite-type ferroelectrics. The maximum value of P_n component in PT is larger than that in BT, probably because bulk PT has larger polarization (86.7 $\mu C/cm^2$) [20] than BT (29.9 $\mu C/cm^2$).

To compensate the restriction of supercell size in first-principles calculations, we further perform complementary phase-field simulations to model the domain wall at a scale of hundreds of nanometers. The results are shown in Fig. 3(b). P_n component exhibits tail-to-tail-like distribution inside the domain wall and converges to zero within 2 nm away from the center of the domain wall, which is in agreement with the DFT calculations. Moreover, the value of the Néel-like component

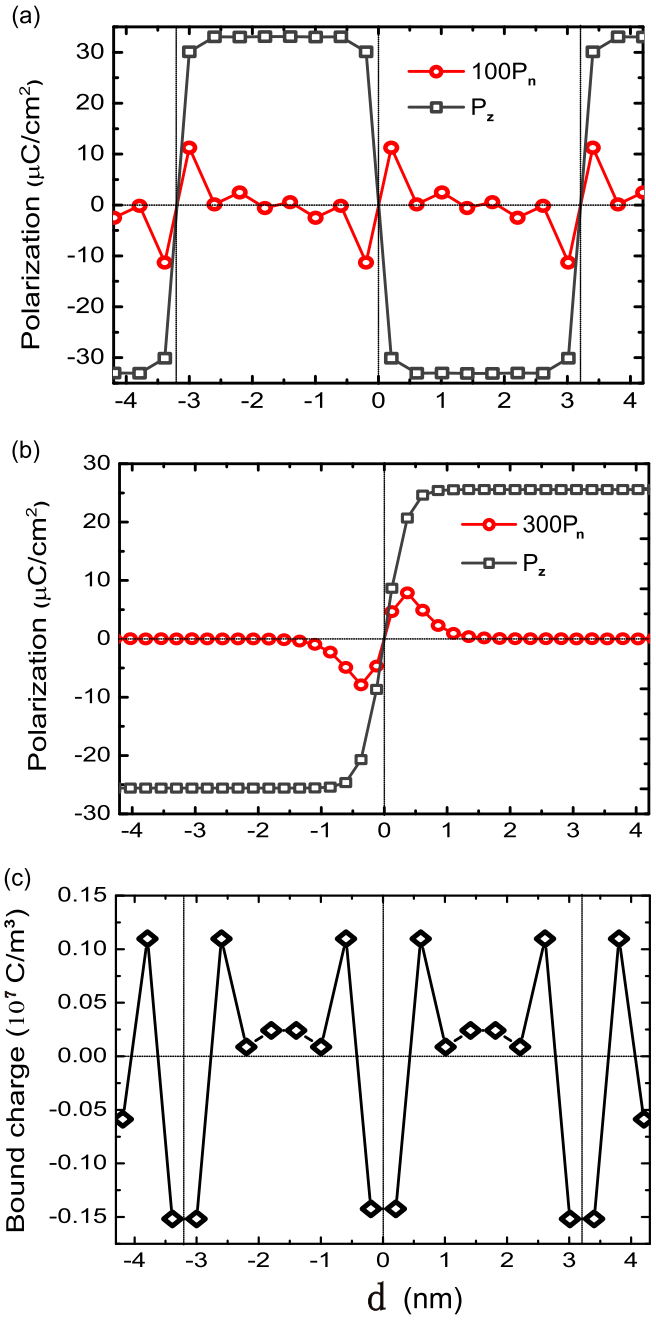

FIG. 3. (Color online) (a) Polarization profile for BaO-centered (100)-FDW from first-principles calculations. Herein d is the distance away from the central BaO plane of the domain wall (i.e., the center of the supercell denoted by the vertical line at $d = 0$). (b) Polarization profile for BaO-centered (100)-FDW from phase-field simulations. (c) Bound charge distribution calculated from P_n component in (a).

from GLD theory is about one third of the value from DFT calculations. Considering the limitations of the two methods, i.e., the ignorance of the high order polarization gradient terms and nonlinear elasticity term in phase-field simulations and the finite-size effect in DFT calculations, the results show qualitative consistency. According to DFT results, P_n and local strain are both small and thus most of the unit cells in the domain structure are not supposed to undergo a sizable distortion from the tetragonal structure.

The reversal of P_n across the domain wall brings about large bound charge. The bound charge can be obtained from the polarization as $\rho^{\text{bound}} = -\nabla \mathbf{P}$ ($\rho^{\text{bound}} = -\frac{\partial}{\partial x}\mathbf{P}_n$ in the present case). The obtained bound charge profile is illustrated in Fig. 3(c). The tail-to-tail-like polarization distribution of the atomic layers within the FDW leads to a negatively charged inner layer and a positively charged outer layer. The charge density of the negatively charged atomic layer is -1.5×10^6 C/m^3 and the positive charge density of the outer layer is about 1×10^6 C/m^3. In contrast to other regions where the bound charge density is an order of magnitude smaller, the FDW could be regarded as a charge multilayer structure which has much stronger interaction with charged dopants. This clearly explains why charged defects, including oxygen vacancies, are easy to be trapped in the domain wall [55], which leads to the pinning effect.

B. 180° (410)-FDW

A previous study based on Ginsburg-Landau-Devonshire theory predicted that FDWs at an angle of around $\pi/12$ have more obvious Bloch-like character [25]. We therefore choose to study the (410)-FDW with the angle [between the (410)-FDW and the (100) lattice plane] of about 14° or −76°. Calculated domain wall energies are given in Table III, while polarization profiles and bound charge of the FDWs are shown in Fig. 4.

From Table III it is clear that the domain wall energy of the (410)-FDW is close to that of the BaO-centered (100)-FDW. This corroborates that the 180° FDW in BT has no preferred orientation [31]. The (410)-FDW energetically favors to center on the BaO plane, as shown in Table III. However, the domain wall energy for TiO-centered FDW is only 20 mJ/m^2 higher than BaO-centered FDW, in contrast with (100)-FDWs, which has an energy difference of 70 mJ/m^2 between TiO-centered and BaO-centered configurations. This difference is easy to understand in terms of domain wall motion barriers. Since 180° FDW is the most stable when lying on the BaO plane, it has to overcome an energy barrier when it moves from one BaO plane to another BaO plane. The farther away the 180° FDW is from its equilibrium position, the higher the energy is. The distance between the (100) BaO plane and its closest TiO plane is $a/2$, while this distance is shortened to $a/2\sqrt{17}$ (about 24% of the former) along the [410] orientation. So it is not surprising that the energy difference between BaO-centered and TiO-centered (100)-FDW is 3.5 times the difference in (410)-FDW structure. Yet similar to the (100)-FDW, TiO-centered and BaO-centered (410)-FDWs have nearly identical polarization profile. It is evident that the center plane does not affect the nature of the domain wall.

Figure 4(a) shows the polarization profile of the (410)-FDW. It can be seen that the P_z component simply reverses its direction within one atomic layer and reduces to zero in the center of the wall, similar to the case of (100)-FDW. However, the P_t and P_n components are both nonzero. The P_n component, i.e., the Néel-like component, despite of its small oscillation away from domain wall area, exhibits a tail-to-tail feature and reaches its maximum value just about 1 Å away from the wall center. While the newly emerged Bloch-like component P_t is even several times larger than

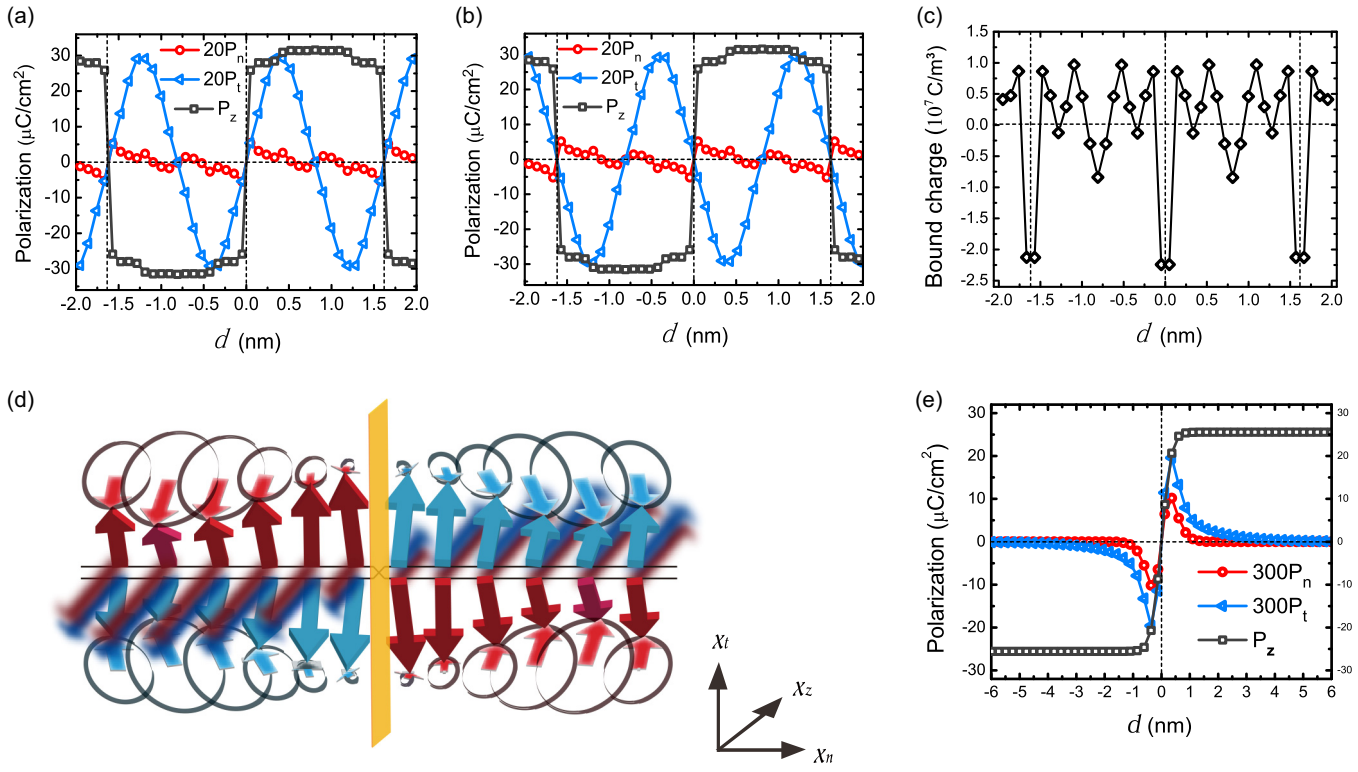

FIG. 4. (Color online) (a) Polarization profile for the BaO-centered (410)-FDW. Herein d is the distance away from the central BaO plane of the domain wall (i.e., the center of the supercell denoted by the vertical line at $d = 0$). The corresponding polarization profile for the $(4\bar{1}0)$-FDW are plotted in (b) as comparisons. (c) Bound charge calculated from the P_n component for the (410)-FDW. (d) Schematic plot of polarizations of (410)-FDW (blue) and $(4\bar{1}0)$-FDW (red). Arrows in the circles are the polarizations projected onto the (001) plane. (e) Polarization profile from phase-field simulations for the domain wall which lies in a plane with an angle of 14° with respect to the (100) plane. This domain wall is equivalent to the (410)-FDW.

the P_n component. The P_t seems to show a sine distribution with the period being half of the supercell length along the x_n direction. But this is not necessarily true because the supercell dimension is limited. How far the P_t component could converge to zero is thus not clear merely judging from Fig. 4(a). It is well known that the phase-field model can simulate the ferroelectric structures at nanometer or even micron scale. Therefore, phase-field simulations are conducted to qualitatively characterize the polarization distribution in the (410)-FDW. The phase-field results in Fig. 4(e) manifest that the Bloch-like component (i.e., P_t) vanishes to zero nearly 3 nm from the center, meaning that the "Bloch wall" is at least 6 nm wide. Although the magnitudes of P_t and P_n are much smaller than the data from DFT calculations, the discrepancy may come from the limitation of the continuum GLD theory, i.e., the higher order polarization gradient terms or nonlinear elasticity may become important at such small scale (within a domain wall width), and the limited supercell dimension in DFT calculations. But the antiferroelectriclike distributions show qualitative agreement.

According to the polarization profile, the maximum value of P_t is 1.47 μC/cm^2, a huge value in comparison with the result of 0.07 μC/cm^2 from Landau theory [25]. In local areas, the total polarization vector deviates from the spontaneous polarization axis of the tetragonal phase by up to 3°. This polarization deviation would not appear in an equal-sized single domain even with random initial atomic displacements. Although the tetragonal atomic configuration is approximately kept in the whole domain wall, the area within two unit cells around the FDW center can be better described by a new structure with the axial angles around $90 \pm 3°$. This deformation around the domain wall may be the main reason for the abnormally high maximal value of the Bloch-like component observed here. As one can see, the existence of the FDW indeed changes atomic positions via coupling between polarization gradient and stress, resulting in a strong distortion of the local structure. However, this structural distortion driven by polarization gradient is short ranged and almost vanishes at 4 Å away from the FDW center.

The $(4\bar{1}0)$ crystallographic plane is related to the (410) plane by a reflection operation about a {100} plane or {110} plane. In BT with no defect, they are equivalent. The existence of the FDWs, however, may break this symmetry. Therefore, we also perform calculations for $(4\bar{1}0)$-FDW to identify the relationship between the $(4\bar{1}0)$-FDW and (410)-FDW. The calculated polarization profile for the $(4\bar{1}0)$-FDW is shown in Fig. 4(b). Comparing Figs. 4(b) and 4(a), one can see that the polarization profiles are quite similar except for the direction of the Bloch-like component P_t. This is totally consistent with the structures of the two FDWs. Actually if projected on a (001) plane, $(4\bar{1}0)$-FDW is the mirror reflection about the center plane of the (410)-FDW. The P_t component is related to atomic displacements along the x_t direction which is changed under the reflection. Thus the left region and right region of the

odd P_t curve get exchanged, ending with sign change of the whole curve from the (410)- to (4$\bar{1}$0)-FDW. In contrast, the x_n direction is normal to the mirror plane and unchanged through the reflection, so the Néel-like component corresponding to atomic displacements along this direction will be the same in the two configurations. Besides, the P_z (Ising) component hardly deviates from the initial setting, indicating that the three polarization components are independent. Figure 4(d) schematically shows the local polarizations within FDW area, where the mirror reflection from the (410)-FDW to (4$\bar{1}$0)-FDW can be clearly seen for the polarization projected on the (001) plane.

Previous simulations based on both first-principles calculations and the GLD model by Taherinejad *et al.* [24] showed that R 180° {1$\bar{1}$0}-FDWs in rhombohedral (R) BT can also be of Ising-type with Bloch-like components. However, they are significantly different from the FDWs in tetragonal (T) phase. First of all, the most stable configuration of R 180° {1$\bar{1}$0}-FDWs is not the mixed Ising-Bloch-like one. First-principles calculations yield an equilibrium traditional Bloch configuration of R 180° {1$\bar{1}$0}-FDWs with the polarization rotation on the (1$\bar{1}$0) plane [24]. But tetragonal 180° (410)-FDW does not have a Bloch solution. The structure characteristics of these two ferroelectric phases can account for the difference. In rhombohedral phase the polar axis has six equivalent orientations, namely along the six body diagonals. When the polarization turns from one diagonal to the opposite direction, it could go through an intermediary diagonal with little structural distortion. But this is not the case in tetragonal phase since the spontaneous polarization can only along the [001] or [00$\bar{1}$] directions. The rotation of the polarization, which can cause a large strain, is costly to happen. Second, the Bloch-like component and Ising component exhibit similar variation trend in R 180° Ising-Bloch-like FDW. The Bloch-like component does not change its direction as long as the Ising component does not, which shows an obvious dependence. But in tetragonal phase, the Bloch-like component changes its magnitude and direction within one domain where the Ising component remains untouched. This phenomenon indicates the robustness of the Ising character of tetragonal 180° FDW, suggesting that the Bloch oblique is only a perturbation and hence relatively independent.

Finally, the bound charge is also deduced from first-principles results using the same expression as for (100)-FDW. We only show the bound charge of (410)-FDW in Fig. 4(c) now that the Néel-like components are exactly alike in (410)- and (4$\bar{1}$0)-FDWs. Since the maximal polarization of Néel-like component at the domain wall is several times larger than that in (100)-FDW, the induced layer charge densities are also magnified a few times. The highest layer charge density is -2.1×10^7 C/m^3 compared to -0.15×10^7 C/m^3 for the (100)-FDW. Therefore, we can infer that (410)-FDW is easier than (100)-FDW to capture charged defects and impurities. Evidently, though being energetically equivalent, 180° FDWs lying on different planes have distinct strength of pinning effect, as long as their Néel-like components vary.

V. CONCLUSION

We have performed first-principles calculations and phase-field simulations for the 180° FDWs in $BaTiO_3$. The domain wall energies, widths, and polarization profiles are obtained for both (100)-FDW and (410)-FDW. It is found that the BaO-centered FDWs are generally more stable than TiO-centered ones, but the polarization nature of the domain wall does not depend on which plane the FDW is centered at. The (100)-FDW shows mixed Ising-Néel-like character, where the "Néel wall" is ~2 nm thick, in agreement with experimental observation [12] and Landau theory prediction [54]. In contrast, the (410)-FDW is revealed to exhibit unique mixed Ising-Bloch-Néel-like character, where the Bloch-like component is not only much larger than the Néel-like component, but also much more extended [our phase-field simulations yield a "Bloch wall" ~6 nm thick for the (410)-FDW]. The stress associated with the polarization gradient is at an oblique angle with the high symmetry directions in the (410)-FDW, which eventually gives rise to its unique polarization characteristics. In addition, the Néel-like polarization component leads to a charge multilayer structure and thus stronger pinning effect of charged defects at the 180° FDWs in $BaTiO_3$.

With analogy to (410)-FDW, most 180° FDWs can show mixed Ising-Néel-Bloch-like character, but the magnitudes of three polarization components vary as the domain wall rotates. Therefore, 180° FDWs along different directions have different widths and bound charge densities, thus resulting in different abilities to trap defects/impurities and diverse behaviors upon external field. In this sense, the wall orientation of 180° FDWs can play an important role in ferroelectric device response. Therefore, it is an interesting subject to explore the dependence of domain wall conductivity, dynamics, defect evolution, etc. on the orientation of 180° FDW. Since BT is a stereotype of ferroelectric perovskites, our findings may be applicable to other ferroelectrics in ABO_3 family, even composite ferroelectrics.

ACKNOWLEDGMENTS

This work was supported by the NSF through Grants DMR-0820404, DMR-1006541, and DMR-1210588 and in part by the China Scholarship Council. The computer simulations were carried out on the LION and cyberstar clusters at the Pennsylvania State University, in part supported by instrumentation (cyberstar Linux cluster) funded by the NSF through Grant OCI-0821527, and the "Explorer 100" cluster system at Tsinghua University. M.L. and W.D. acknowledge the support from the Ministry of Science and Technology of China (Grants No. 2011CB921901 and No. 2011CB606405), and the National Natural Science Foundation of China.

[1] W. Kanzig, Solid State Phys.: Adv. Res. Appl. **4**, 1 (1957).
[2] O. Auciello, J. F. Scott, and R. Ramesh, Phys. Today **51**, 22 (1998).
[3] M. Dawber, K. Rabe, and J. Scott, Rev. Mod. Phys. **77**, 1083 (2005).
[4] J. Scott, Science **315**, 954 (2007).

[5] D. G. Schlom, L. Q. Chen, C. B. Eom, K. M. Rabe, S. K. Streiffer, and J. M. Triscone, Annu. Rev. Mater. Res. **37**, 589 (2007).

[6] D. Damjanovic, Rep. Prog. Phys. **61**, 1267 (1998).

[7] T. J. Yang, V. Gopalan, P. J. Swart, and U. Mohideen, Phys. Rev. Lett. **82**, 4106 (1999).

[8] T. Tybell, P. Paruch, T. Giamarchi, and J. M. Triscone, Phys. Rev. Lett. **89**, 097601 (2002).

[9] Y.-H. Shin, I. Grinberg, I. W. Chen, and A. M. Rappe, Nature (London) **449**, 881 (2007).

[10] S. V. Kalinin, A. N. Morozovska, L. Q. Chen, and B. J. Rodriguez, Rep. Prog. Phys. **73**, 056502 (2010).

[11] E. A. Eliseev, A. N. Morozovska, G. S. Svechnikov, E. L. Rumyantsev, E. I. Shishkin, V. Y. Shur, and S. V. Kalinin, Phys. Rev. B **78**, 245409 (2008).

[12] C. L. Jia, S. B. Mi, K. Urban, I. Vrejoiu, M. Alexe, and D. Hesse, Nat. Mater. **7**, 57 (2008).

[13] J. Seidel, L. W. Martin, Q. He, Q. Zhan, Y. H. Chu, A. Rother, M. E. Hawkridge, P. Maksymovych, P. Yu, M. Gajek *et al.*, Nat. Mater. **8**, 229 (2009).

[14] S. Farokhipoor and B. Noheda, Phys. Rev. Lett. **107**, 127601 (2011).

[15] J. Guyonnet, I. Gaponenko, S. Gariglio, and P. Paruch, Adv. Mater. **23**, 5377 (2011).

[16] J. F. Scott and M. Dawber, Appl. Phys. Lett. **76**, 3801 (2000).

[17] L. He and D. Vanderbilt, Phys. Rev. B **68**, 134103 (2003).

[18] N. Church, J. M. Feinberg, and R. Harrison, Geochem. Geophys. Geosyst. **12**, Q07z27 (2011).

[19] J. Padilla, W. Zhong, and D. Vanderbilt, Phys. Rev. B **53**, R5969 (1996).

[20] D. Lee, R. K. Behera, P. Wu, H. Xu, Y. L. Li, S. B. Sinnott, S. R. Phillpot, L. Q. Chen, and V. Gopalan, Phys. Rev. B **80**, 060102 (2009).

[21] V. R. Aravind, A. N. Morozovska, S. Bhattacharyya, D. Lee, S. Jesse, I. Grinberg, Y. L. Li, S. Choudhury, P. Wu, K. Seal *et al.*, Phys. Rev. B **82**, 024111 (2010).

[22] D. Lee, H. Xu, V. Dierolf, V. Gopalan, and S. R. Phillpot, Phys. Rev. B **82**, 014104 (2010).

[23] R. K. Behera, C. W. Lee, D. Lee, A. N. Morozovska, S. B. Sinnott, A. Asthagiri, V. Gopalan, and S. R. Phillpot, J. Phys.: Condens. Matter **23**, 175902 (2011).

[24] M. Taherinejad, D. Vanderbilt, P. Marton, V. Stepkova, and J. Hlinka, Phys. Rev. B **86**, 155138 (2012).

[25] P. V. Yudin, A. K. Tagantsev, E. A. Eliseev, A. N. Morozovska, and N. Setter, Phys. Rev. B **86**, 134102 (2012).

[26] Z. Wu, N. Huang, Z. Liu, J. Wu, W. Duan, B.-L. Gu, and X.-W. Zhang, Phys. Rev. B **70**, 104108 (2004).

[27] Z. Wu, N. Huang, J. Wu, W. Duan, and B.-L. Gu, Appl. Phys. Lett. **86**, 202903 (2005).

[28] J. Yu, Z. Wu, Z. Liu, Q. Yan, J. Wu, and W. Duan, J. Phys.: Condens. Matter **20**, 135203 (2008).

[29] Here the Bloch-like and Néel-like characters should be distinguished from the original meaning in magnetic domain wall because of the facts that the observed P_n and P_t profiles have different symmetry from the original Néel and Bloch profiles and relatively small values compared to the spontaneous polarization.

[30] M. H. Frey and D. A. Payne, Phys. Rev. B **54**, 3158 (1996).

[31] Z.-X. Chen, Y. Chen, and Y.-S. Jiang, J. Phys. Chem. B **105**, 5766 (2001).

[32] J. J. Wang, F. Y. Meng, X. Q. Ma, M. X. Xu, and L. Q. Chen, J. Appl. Phys. **108**, 034107 (2010).

[33] B. Meyer and D. Vanderbilt, Phys. Rev. B **65**, 104111 (2002).

[34] I. Dawson, P. D. Bristowe, M. H. Lee, M. C. Payne, M. D. Segall, and J. A. White, Phys. Rev. B **54**, 13727 (1996).

[35] P. Marton, T. Shimada, T. Kitamura, and C. Elsasser, Phys. Rev. B **83**, 064110 (2011).

[36] G. Kresse and J. Furthmüller, Phys. Rev. B **54**, 11169 (1996).

[37] G. Kresse and D. Joubert, Phys. Rev. B **59**, 1758 (1999).

[38] P. E. Blöchl, Phys. Rev. B **50**, 17953 (1994).

[39] J. P. Perdew, K. Burke, and M. Ernzerhof, Phys. Rev. Lett. **77**, 3865 (1996).

[40] We have done some test calculations by either switching off the symmetry during the ionic relaxation or manually breaking the existent symmetry. For the (100)-FDW with a high symmetry, releasing the symmetry constraints leads to some small artificial polarization components, but the overall trend is not affected. Besides, the structure with symmetry constraints is more stable than the testing structures. For the (410)-FDW of which symmetry is lower than the (100)-FDW, the resultant structures unconfined by symmetry hardly deviate from the symmetry-constrained optimized structure.

[41] W. Press, B. Flannery, S. Teukolsky, and W. Vetterling, *Numerical Recipes in C: The Art of Scientific Computing* (Cambridge University Press, Cambridge, UK, 1992).

[42] M. C. Payne, M. P. Teter, D. C. Allan, T. Arias, and J. Joannopoulos, Rev. Mod. Phys. **64**, 1045 (1992).

[43] M. Gajdoš, K. Hummer, G. Kresse, J. Furthmüller, and F. Bechstedt, Phys. Rev. B **73**, 045112 (2006).

[44] L.-Q. Chen, Annu. Rev. Mater. Res. **32**, 113 (2002).

[45] E. A. Eliseev, A. N. Morozovska, M. D. Glinchuk, and R. Blinc, Phys. Rev. B **79**, 165433 (2009).

[46] J. Wang, P. Wu, X. Ma, and L. Chen, J. Appl. Phys. **108**, 114105 (2010).

[47] G. Rupprecht and R. Bell, Phys. Rev. **135**, A748 (1964).

[48] J. Hlinka and P. Marton, Phys. Rev. B **74**, 104104 (2006).

[49] R. Maranganti and P. Sharma, Phys. Rev. B **80**, 054109 (2009).

[50] A. G. Khachaturyan, *Theory of Structural Transformations in Solids* (Dover, Mineola, NY, 2008).

[51] G. Shirane, H. Danner, and R. Pepinsky, Phys. Rev. **105**, 856 (1957).

[52] C. J. Xiao, C. Q. Jin, and X. H. Wang, Mater. Chem. Phys. **111**, 209 (2008).

[53] G. Kwei, A. Lawson, S. Billinge, and S. Cheong, J. Phys. Chem. **97**, 2368 (1993).

[54] M. Y. Gureev, A. K. Tagantsev, and N. Setter, Phys. Rev. B **83**, 184104 (2011).

[55] C. H. Park and D. J. Chadi, Phys. Rev. B **57**, R13961 (1998).